Inorg. Chem. **2007**, *46*, 5093–5099

Single-Phase Titania Nanocrystallites and Nanofibers from Titanium Tetrachloride in Acetone and Other Ketones

Yu Wu,[†] Hong-Mei Liu,[†] Bo-Qing Xu,*[,†] Zao-Li Zhang,[‡] and Dang-Sheng Su[‡]

Innovative Catalysis Program, Key Lab of Organic Optoelectronics & Molecular Engineering, Department of Chemistry, Tsinghua University, Beijing 100084, China, and Inorganic Chemistry Department, Fritz Haber Institute of the Max Planck Society, Faradayweg 4-6, 14195 Berlin, Germany

Received February 3, 2007

Single-phase titania nanomaterials were prepared by autoclaving titanium tetrachloride in acetone at 80–140 °C. Depending on the molar ratio of $TiCl_4$ to acetone ($TiCl_4$/Ac), TiO_2 materials with different phases and morphologies were obtained. When the $TiCl_4$ concentration was no higher than $TiCl_4$/Ac = 1/15, single-phase anatase TiO_2 nanocrystals in sizes ranging from 4 to 10 nm were prepared by tuning $TiCl_4$/Ac ratios from 1/90 to 1/15. However, when the $TiCl_4$ concentration was high enough (e.g., $TiCl_4$/Ac ≥ 1/10), single-phase rutile TiO_2 nanofibers were obtained selectively. The materials were characterized comprehensively using X-ray diffraction, transmission electron microscopy, Raman spectroscopy, thermogravimetric analysis, and nitrogen adsorption measurements. With the aid of GC/MS analysis of organic products in the liquid phase, it is shown that the controlled hydrolysis of $TiCl_4$ with water, which was in situ generated from the $TiCl_4$-catalyzed aldol condensation reactions of acetones, played an important role in the formation of the titania nanomaterials. Some of the organic condensates may function to stabilize the phase and morphology of the materials. This mechanism was also supported by our success in using other ketones as alternatives to acetone in the synthesis.

1. Introduction

Because of the importance in many key technologies of titania-based nanomaterials, synthesis of highly crystalline titania nanoparticles with controlled size, morphology, and crystal structure has been an important research focus in the field of materials chemistry.[1] Colvin et al.[2] were the first to prepare small anatase nanocrystallites (3.8−9.2 nm) by reacting titanium halides with titanium alkoxides at 300 °C using a nonaqueous solvent (e.g., heptadecane) in the presence of an additive (e.g., trioctylphosphine (TOPO)), which stimulated interest in nonaqueous approaches to control of the size distribution, morphology, and crystal phase of TiO_2 nanomaterials. By reacting $TiCl_4$ in various alcohol homologues in the presence or absence of acetic acid, Li et al. succeeded in obtaining TiO_2 nanocrystallites varying in crystal phase (rutile or anatse) and morphology (spherical, fiberlike, or rodlike).[3] However, it was not clear whether it could be possible to manipulate the crystal phase and morphologies of TiO_2 nanocrystallites using a single alcohol source. Alternatively, Niederberger et al.[4] obtained highly crystalline TiO_2 nanoparticles by reacting $TiCl_4$ in benzyl alcohol at low temperature (40 °C), and with proper control of the later thermal processing conditions, the product particle sizes were found tunable in the range of 4−8 nm. Woodfield et al. even produced high-purity anatase nanoparticles by proper calcination of the reaction product of $TiCl_4$ in ethanol.[5] In the presence of a proper organic additive (amine or oleic acid), carefully controlled hydrolysis of titanium tetraisopropoxide in carboxylic acids was found to produce

* To whom correspondence should be addressed. E-mail: bqxu@tsinghua.edu.cn.
[†] Tsinghua University.
[‡] Fritz Haber Institute of the Max Planck Society.

(1) (a) Linsebigler, A. L.; Lu, G. Q.; Yates, J. T. *Chem. Rev.* **1995**, *95*, 735. (b) O'Regan, B.; Grtzel, M. *Nature* **1991**, *353*, 737. (c) Wang, H.; Wu, Y.; Xu, B. Q. *Appl. Catal., B* **2005**, *59*, 139.
(2) Trentler, T. J.; Denler, T. E.; Bertone, J. F.; Agrawal, A.; Colvin, V. L. *J. Am. Chem. Soc.* **1999**, *121*, 1613.
(3) (a) Wang, C.; Deng, Z. X.; Li, Y. *Inorg. Chem.* **2001**, *40*, 5210. (b) Wang, C.; Deng, Z. X.; Zhang, G.; Fan, S.; Li, Y. *Powder Technol.* **2002**, *125*, 39.
(4) (a) Niederberger, M.; Bartl, M. H.; Stucky, G. D. *Chem. Mater.* **2002**, *14*, 4364. (b) Niederberger, M.; Bartl, M. H.; Stucky, G. D. *J. Am. Chem. Soc.* **2002**, *124*, 13642.
(5) Li, G. S.; Li, L. P.; Boerio-Goates, J.; Woodfiled, B. F. *J. Am. Chem. Soc.* **2005**, *127*, 8659.

10.1021/ic070199h CCC: $37.00
Published on Web 05/15/2007

macroporous TiO_2 microspheres[6] or high-aspect-ratio anatase TiO_2 nanorods.[7] These studies further demonstrate the interesting prospect of the nonaqueous approaches for the synthesis of diversified TiO_2-based materials.

The nonaqueous approaches mentioned above were extended very recently to non-alcohol/non-hydroxyl oxygen-containing organic solutions by Niederberger et al.,[8] who showed that reactions between titanium tetraisopropoxides and ketones or aldehydes at 130 °C could result in anatase TiO_2 nanocrystallites of ca. 15 nm. The use of ketone or aldehyde as the organic reagent was a significant advance because it directly produced anatase TiO_2 nanocrystals without the need for any special additive or template.[3,9] It would be of great interest to explore any possibility of manipulating the crystal phase and morphology of TiO_2 nanocrystallites using an inorganic titanium salt and a single organic source or in the absence of any special additive or template.

We report herein that, without the use of any additive, single-phase anatase TiO_2 nanocrystallites with small, uniform, and yet tunable sizes between 4 and 10 nm can be selectively synthesized simply by autoclaving a $TiCl_4$/acetone mixture of proper $TiCl_4$ concentration at fairly low temperature (80−140 °C). By a simple increase in the concentration of $TiCl_4$, the present method can also be manipulated to produce needlelike single-phase rutile TiO_2 fibers of ca. 10 nm widths. Autoclaving $TiCl_4$ in other aldehydes or ketones capable of performing aldol condensation reactions is shown to produce similar TiO_2 nanomaterials.

2. Experimental Section

2.1. Preparation. The procedure for the synthesis of TiO_2 nanomaterials is as follows. Typically, a certain volume of $TiCl_4$ (1.0−9.0 mL) was quickly dropped into a fixed volume of acetone (60 mL) under vigorous stirring at room temperature (**take caution because the reaction is highly exothermic**). The obtained solution was transferred to and sealed in a Teflon-lined autoclave (ca. 100 mL). The autoclave was then placed in an oven for solvothermal treatment at 80−140 °C for 12 h. After the autoclave was cooled in cold water, the dark-red pasty precipitates formed in the autoclave were separated by filtration. Repeated washing of the precipitates with excessive acetone gave dry and loose powder samples, which were used later for different characterizations. Using autoclaves of larger volumes, the present preparation was easily scaled up in our laboratory for production of a 5−10 g TiO_2 sample in a single batch of the synthesis.

2.2. Characterizations. Powder X-ray diffraction (XRD) measurements were performed on a Bruker D8 Advance X-ray diffractometer, using a monochromatized Cu Kα (λ = 1.5418 Å) radiation source. The average crystallite size (d, in nanometers) of each TiO_2 sample was obtained from X-ray line-broadening analysis using the well-known Scherrer equation:

$$d = 0.89\lambda/B(2\theta)\cos\theta$$

where $B(2\theta)$ is the width of the XRD peak at half-peak-height in radians, λ is the wavelength of the X-ray in nanometers, and θ is the angle between the incident and diffracted beams in degrees.

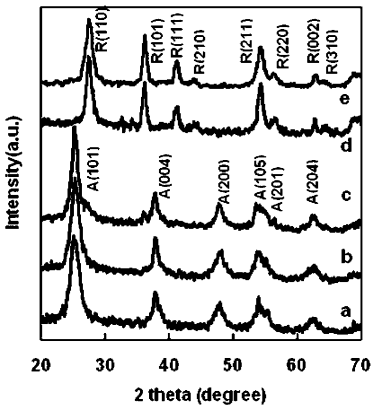

Figure 1. XRD patterns of TiO_2 prepared at 110 °C with molar $TiCl_4$/Ac ratios of 1/90 (a: anatase, 5.3 nm), 1/30 (b: anatase, 6.2 nm), 1/15 (c: anatase, 8.6 nm), 1/10 (d: rutile, 9.9 nm), and 1/7 (e: rutile, 7.8 nm).

Raman spectra were recorded on a Renishaw RM2000 microscopic confocal Raman spectrometer employing a 514 nm laser beam. The size and morphology of the materials were measured on a JEOL JEM-2010 transmission electron microscope, equipped with an Oxford INCA analyzer. High-resolution transmission electron microscopy (HRTEM) studies were performed on a Philips CM200 LaB6 operating at 200 kV. BET surface areas and pore volumes of the samples were performed with nitrogen adsorption at −196 °C on a Micromeritics ASAP 2010C instrument; the samples were degassed under vacuum at 150 °C for 5 h before the measurements. Thermogravimetric oxidation (TG) measurements were conducted on a Mettler-Toledo DTG/SDTA851 instrument in flowing air (60 mL/min); the samples were heated to 1000 °C with a temperature ramp of 15 °C/min.

3. Results and Discussion

3.1. Product Crystal Phase and Size. Figure 1 shows the effect of the $TiCl_4$ concentration in acetone on the XRD crystal phase structure of the TiO_2 powders obtained with an autoclaving temperature of 110 °C. The concentration is expressed as the $TiCl_4$/Ac molar ratio. The sizes given in the caption of this figure were the average crystallite sizes of the samples calculated by applying the well-known Debye−Scherrer equation to the diffractions of the anatase (1, 0, 1) or rutile (1, 1, 0) planes. The crystal phase and size of the TiO_2 crystals were seen to be dependent on the molar $TiCl_4$/Ac ratio. The crystals obtained with low concentrations of $TiCl_4$, that is, at $TiCl_4/Ac \leq 1/15$, appeared as a pure anatase phase. In contrast, pure rutile TiO_2 samples were produced in the synthesis with higher $TiCl_4$ concentration, as shown by the d and e patterns in Figure 1 for $TiCl_4/Ac = 1/10$ and 1/7, respectively.

We attempted to compare the sample crystallite sizes in different directions by applying the Debye−Scherrer equation to different diffraction lines in the XRD patterns. For the anatase crystals, the sizes according to their (2, 0, 0) diffractions were found to be comparable to those on the

(6) Zhong, Z. Y.; Chen, F. X.; Ang, T. P.; Han, Y. F.; Lim, W. Q.; Gedanken, A. *Inorg. Chem.* **2006**, *45*, 4619.
(7) Cozzoli, P. D.; Kornowski, A.; Weller, H. *J. Am. Chem. Soc.* **2003**, *125*, 14539.
(8) Garnweitner, G.; Antonietti, M.; Niederberger, M. *Chem. Commun.* **2005**, *3*, 397.
(9) Wu, Y.; Liu, H. M.; Xu, B. Q. *Appl. Organomet. Chem.* **2007**, *21*, 146.

Table 1. Features of the TiO_2 Products Obtained Using Varying Reactant Ratios and Autoclaving Temperatures

$TiCl_4$/Ac	reaction temp (°C)	yield (%)	crystal structure	crystallite size[a] (nm)	TEM size[b] (nm)	oxide content[c] (%)	surface area[d] (m^2/g)
1/90	110	95	anatase	5.3	5.4	86.0	201
1/30	110	92	anatase	6.2	6.0	87.0	174
1/15	110	85	anatase	8.6	8.9	88.5	84
1/10	110	53	rutile	9.9 (15.4)	8−12 × 1000	90.0	6
1/7	110	48	rutile	7.8 (13.8)	10−20 × 100−1000	94.5	12
1/90	140	91	anatase	6.9		85.5	163
1/30	140	92	anatase	7.2	7.0	90.0	152
1/10	140	76	rutile	15.3 (25.8)	15−25 × 200−2000	96.0	
1/90	80	92	anatase	3.8		84.5	243
1/30	80	90	anatase	5.6	5.7	86.5	194
1/10	80	ND[e]					

[a] Average crystallite size calculated from the (1, 0, 1) diffraction line of anatase or (1, 1, 0) of rutile samples using the Debye−Scherrer equation. Sizes in parentheses for rutile samples are calculated from their (1, 1, 1) diffraction lines. [b] Particle size from TEM observation. [c] Obtained from TGA measurements of the samples. [d] Measured by nitrogen physisorption using the BET method. [e] No solid products detected.

basis of the (1, 0, 1) diffractions. However, the crystallite sizes of the rutile samples according to their (1, 1, 1) diffractions, that is, crystallite sizes given in the parentheses of Table 1, appeared to be much bigger than those based on the (1, 1, 0) diffractions. These calculations suggest that the anatase crystals assumed a roughly spherical shape, but the rutile ones were shaped differently.

Moreover, the average size of the anatase crystallites (also Table 1) increased with an increase of the $TiCl_4$ concentration in acetone; for example, the average size was 5.3 nm at $TiCl_4$/Ac = 1/90, whereas it became 6.2 and 8.6 nm at $TiCl_4$/Ac = 1/30 and 1/15, respectively. These results indicate that the sizes of the anatase crystallites can be finely tuned by changing the $TiCl_4$ concentration.

We also found that the autoclaving temperature showed a significant effect on the crystallite sizes of the as-prepared anatase nanoparticles (Table 1). When a higher autoclaving temperature (e.g., 140 °C) was used, the average crystallite size of the anatase product became 6.9 nm at $TiCl_4$/Ac = 1/90 and 7.2 nm at $TiCl_4$/Ac = 1/30. When the autoclaving temperature was lowered to 80 °C, the obtained crystallites showed an average size of 3.8 nm at $TiCl_4$/Ac = 1/90 and 5.6 nm at $TiCl_4$/Ac = 1/30, respectively, which are significantly smaller than those obtained at 110 °C. Thus, a higher autoclaving temperature is favorable for the formation of larger anatase crystallites. However, it is noteworthy that the single-phase anatase crystallites obtained in the present $TiCl_4$/Ac system are significantly smaller than those obtained in the titanium tetraisopropoxide/acetone system (ca. 15 nm) reported in ref 8.

Raman spectroscopy was also used to characterize the TiO_2 samples shown in Figure 1. The XRD-pure anatase and rutile crystallites also appeared respectively as single-phase anatase and rutile TiO_2 in the Raman spectra (Figure 2), which further confirms the single-phase feature of the TiO_2 products in our present approach. In comparison with the standard Raman signals, a slight blue shift and broadening occurred for the E_g mode (ca. 153 cm^{-1}) in the Raman spectra of the synthesized anatase samples, which may be due to phonon confinement and strain effects applied by organic residues on the sample surfaces.[10] Thus, our data uncover a low-temperature (80−140 °C) approach for crystal-phase-controlled synthesis of TiO_2 nanocrystals by simply changing the concentration of $TiCl_4$ in acetone.

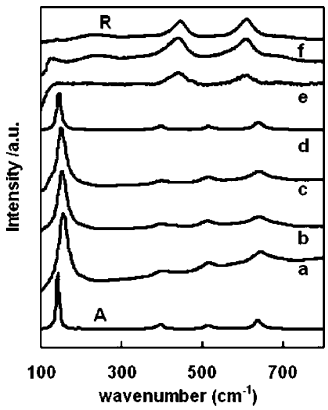

Figure 2. Raman spectra of TiO_2 samples prepared at 110 °C: (a) anatase TiO_2 nanocrystals obtained with $TiCl_4$/Ac = 1/90, (b) anatase TiO_2 nanocrystals obtained with $TiCl_4$/Ac = 1/30, (c) sample (b) after the calcinations at 600 °C, (d) anatase TiO_2 nanocrystals obtained with $TiCl_4$/Ac = 1/15, (e) rutile TiO_2 fibers obtained with $TiCl_4$/Ac = 1/10, and (f) rutile TiO_2 fibers obtained with $TiCl_4$/Ac = 1/7. A and R are the Raman spectra of standard anatase and rutile TiO_2, respectively.

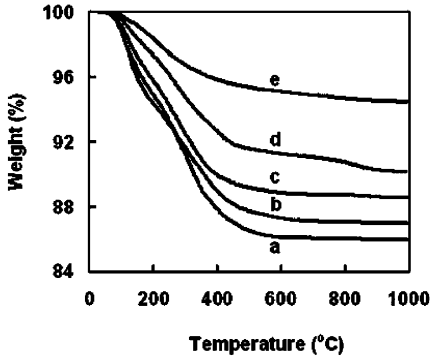

Figure 3. TG results of TiO_2 powders obtained at 110 °C at the reactant with $TiCl_4$/Ac ratios of 1/90 (a), 1/30 (b), 1/15 (c), 1/10 (d) and 1/7 (e).

The single-phase anatase sample with an average crystallite size of 5.3 nm, obtained at $TiCl_4$/Ac = 1/90, was subject to calcination for 3 h at 600 °C in flowing air. A Raman spectrum of the calcined sample (Figure 2c) indicated that the single-phase anatase structure remained unchanged during the calcination, thus demonstrating a high thermal stability of the anatase phase. In addition, the signal for the E_g mode in the Raman spectrum returned to its normal position (ca. 144 cm^{-1}) after the calcination, which can be accounted for by an oxidative elimination of organic residues during the high-temperature calcination.

3.2. Content of Organic Residues and Yield of TiO_2. Thermogravimetric analysis (TGA) in flowing air was conducted to quantify the amount of organic residues (or TiO_2 content) in the prepared TiO_2 materials (Figure 3). The measured weight loss was in the range of 10−15% for the anatase and 4−10% for the rutile samples. It should be

(10) Xu, C. Y.; Zhang, P. X.; Yan, L. J. *Raman Spectrosc.* **2001**, *32*, 862.

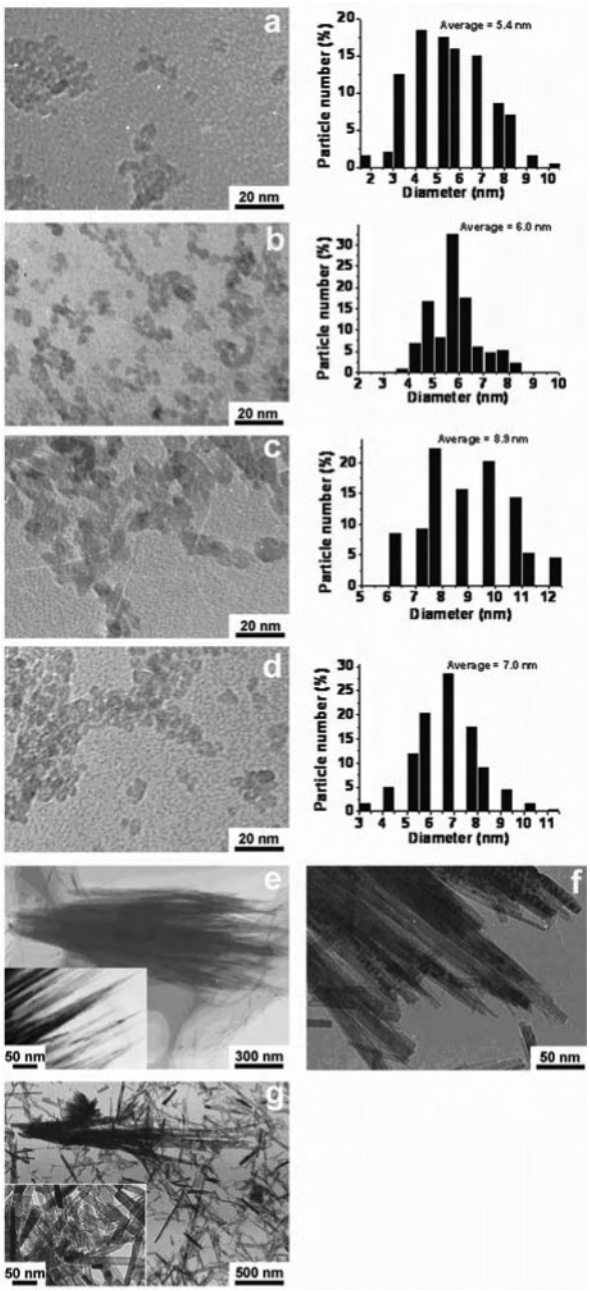

Figure 4. TEM images of TiO_2 samples obtained at different $TiCl_4$/Ac ratios and autoclaving temperatures: (a) $TiCl_4$/Ac = 1/90, 110 °C, (b) $TiCl_4$/Ac = 1/30, 110 °C, (c) $TiCl_4$/Ac = 1/15, 110 °C, (d) $TiCl_4$/Ac = 1/30, 140 °C, (e) $TiCl_4$/Ac = 1/10, 110 °C, (f) $TiCl_4$/Ac = 1/7, 110 °C, and (g) $TiCl_4$/Ac = 1/10, 140 °C. The column graphs to the right of each of the TEM photos were obtained by measuring (a) 261, (b) 235, (c) 214, and (d) 238 crystallites.

notified that the single-phase structure of the materials was not changed after the removal of organic residuals by calcining up to 600 °C in flowing air. Thus, the TiO_2 yield was 85−100% for the production of single-phase anatase crystallites, which is close to those reported in ref 8, but it was only 48−76% for the formation of single-phase rutile materials. As can be seen in Table 1, the yield in producing the rutile TiO_2 can be improved significantly by increasing the autoclaving temperature.

3.3. Product Morphology and Particle Size Distribution. TEM of different resolutions was employed to gain information on the morphology and size distribution of the TiO_2 crystallites. In the TEM images (Figure 4), the anatase materials appeared as uniform irregular particles with sizes that are close to their XRD crystallite sizes (Table 1). Consistent with the average XRD crystallite sizes, the average TEM particle sizes of the anatase products increased also with the $TiCl_4$/Ac ratio and the autoclaving temperature. For instance, the average TEM particle size of the anatase sample obtained at 110 °C increased from 5.4 nm at $TiCl_4$/Ac = 1/90 (Figure 4a) to 6.0 nm at $TiCl_4$/Ac = 1/30 (Figure 4b) and then to 8.9 nm at $TiCl_4$/Ac = 1/15 (Figure 4c). When the synthesis was performed with the ratio fixed at $TiCl_4$/Ac = 1/30, the average TEM particle size was 7.0 nm at 140 °C (Figure 4d) and 5.7 nm at 80 °C (Table 1).

Parts e and f of Figure 4 show the representative TEM images of the rutile crystals obtained by autoclaving at

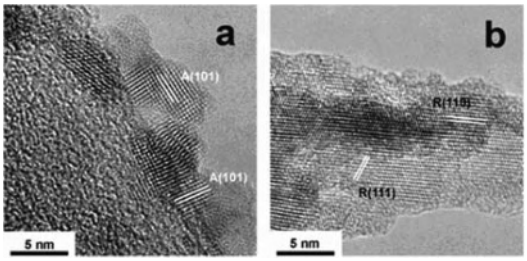

Figure 5. HRTEM images of samples obtained with $TiCl_4$/Ac ratios of (a) 1/30 and (b) 1/10, at 110 °C. A and R denote anatase and rutile, respectively.

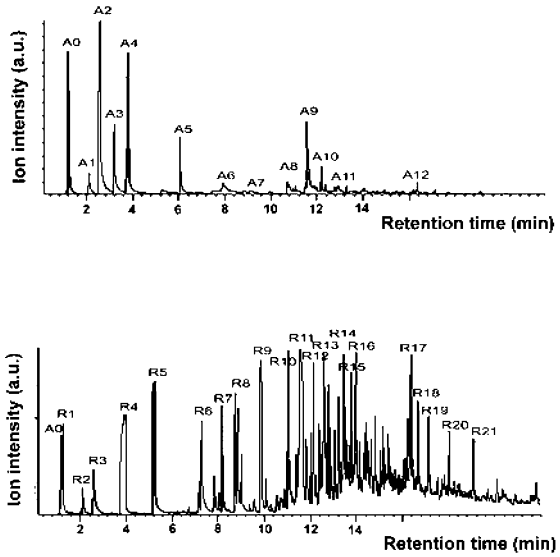

Figure 6. GC/MS plots of liquid products obtained from mixtures of $TiCl_4$/Ac (molar) = 1/30 (up) and $TiCl_4$/Ac = 1/10 (down).

Table 2. Comparison of Different Ketones in the Autoclaving Synthesis of Titania Nanomaterials

ketone	$TiCl_4$/ketone	reaction temp (°C)	yield (%)	crystal structure	crystallite size (nm)
butanone	1/30	110	90	anatase	6.2
4-methylpentanone	1/30	110	89	anatase	5.7
4-methylpentanone	1/10	140	38	rutile	
acetophenone	1/30	110	86	anatase	8.8

Scheme 1[a]

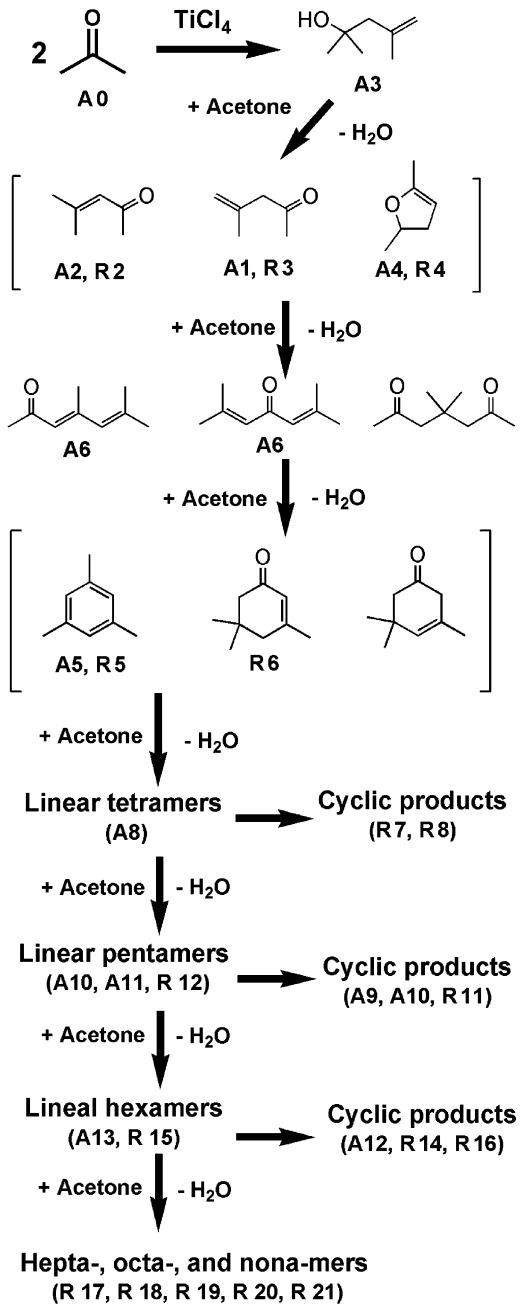

[a] Possible reactions leading to the GC/MS-detected organics from the $TiCl_4$/Ac mixtures. **A0**, **A1**, **A2**, ..., **A*n*** denote the organics detected in the liquids separated from the anatase products, whereas **R1**, **R2**, ..., **R*n*** refer to those separated from the rutile nanofibers (Figure 6).

110 °C mixtures of $TiCl_4$/Ac = 1/10 and $TiCl_4$/Ac = 1/7, respectively. The rutile materials obtained with the mixture of $TiCl_4$/Ac = 1/10 appeared as bundles of needlelike fibers with sizes of ca. 8−12 nm × 1000 nm, and the product obtained with a slightly higher $TiCl_4$/Ac ratio ($TiCl_4$/Ac = 1/7) showed a fibrous or rodlike morphology of ca. 10−20 nm × 100−1000 nm. Figure 4g presents images of the rutile crystals produced by autoclaving the mixtures of $TiCl_4$/Ac = 1/10 at 140 °C, which contains mainly fibrous TiO_2 of ca. 15−25 nm × 200−2000 nm. These observations further indicate that, even for the synthesis of the fibrous single-phase rutile material, the $TiCl_4$ concentration as well as the reaction temperature would subtly affect the product size and morphology.

Table 3. Some Low Molecular Weight Chlorine-Containing Organics Detected in the Liquid Phase

	low $TiCl_4$ concentration systems	high $TiCl_4$ concentration systems		
chlorine-containing organics	**A7**	**R1**	**R9**	**R13**
molecular formula	$C_{12}H_{17}Cl$	C_3H_7OCl	$C_{12}H_{17}Cl$	$C_{15}H_{23}OCl$
molecular (*m*/*e*)	196	94	196	254

HRTEM images shown in Figure 5 clearly indicate that the anatase TiO_2 nanoparticles and rutile TiO_2 nanofibers are highly crystallized (Figure 5a). HRTEM images of the fibers (Figure 5b) are indicative of single-crystalline fibers, which were probably formed by epitaxial crystal growth. It is therefore very clear that the change in the $TiCl_4$ concentration in acetone is feasible for control of the crystal phase and morphology of the TiO_2 materials.

The data presented above show a novel low-temperature solvothermal synthetic approach enabling highly flexible manipulation of the crystal phase, size, and morphology of TiO_2 nanomaterials with the same reactant sources ($TiCl_4$ and acetone) and, very importantly, with no need for any additional surfactant or template. In view of economics, titanium halides are much cheaper than alkoxides, which makes the present findings more attractive in producing advanced TiO_2 nanomaterials with well-selected crystal phase, size, and morphology.

3.4. Synthesis with Alternative Ketones. To understand if acetone is specific in inducing the size, morphology, and phase formation of TiO_2 nanomaterials, we also performed similar syntheses by replacing acetone with several other ketones including butanone, 4-methylpentanone, and acetophenone. These syntheses were done at 110 °C at a fixed reactant molar ratio of $TiCl_4$/ketone = 1/30. Table 2 compares the product features using these alternative ketones. Again, we see the formation of small (<10 nm) single-phase anatase crystals in good yield (85−90%) for each of the selected ketones. When the synthesis was performed with a high $TiCl_4$ concentration (e.g., $TiCl_4$/ketone = 1/10) at 140 °C, we also obtained fibrous single-phase rutile materials. Specifically, an autoclaving of the mixture of $TiCl_4$/4-methylpentanone = 1/10 at 140 °C resulted in the production of fibrous rutile crystals with dimensions of 15−25 nm × 200−2000 nm. Thus, our method could be developed as a general approach for syntheses of advanced TiO_2 nanomaterials.

3.5. Nature of Organic Products and Possible Mechanism of TiO_2 Formation. To gain insight into the mechanism of nanocrystal formation in the present approach, we analyzed with GC/MS the nature of the liquid products separated from the solids. A broad spectrum of organic compounds with molecular weights of up to and higher than 300 were detected, and the majority were identified as dehydrated products of the intermolecular aldol condensation of acetone (Figure 6 and Scheme 1).[11] In the syntheses of

(11) Paulis, M.; Martin, M.; Soria, D. B.; Diaz, A.; Odriozola, J. A.; Montes, M. *Appl. Catal., A* **1999**, *180*, 411.

Scheme 2 [a]

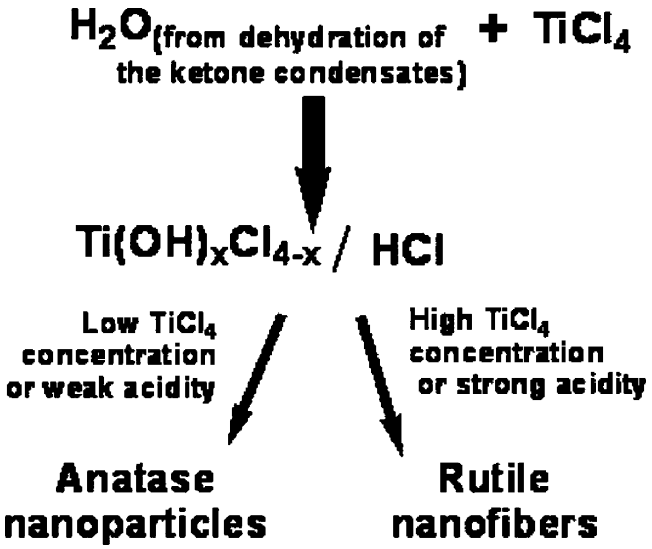

[a] Influence of the $TiCl_4$ concentration in ketones on the crystallite structure and morphology of TiO_2.

the anatase materials with low $TiCl_4$ concentrations (i.e., $TiCl_4$/Ac $\leq$ 1/15), the detected organic products were basically free of chlorine; only a trace amount of chlorine-containing **A7** was detected (Figure 6), whereas in the syntheses of the rutile fibers with higher $TiCl_4$ concentrations (e.g., $TiCl_4$/Ac = 1/10), significant quantities of chlorine-containing organics were detected (Table 3). The hardly detected chlorine-containing organics in the liquids separated from the single-phase anatase materials are distinct from the non-hydrolytic sol−gel synthesis of small anatase TiO_2 nanocrystallites (3.8−9.2 nm) reported earlier by Colvin et al.,[2] who reacted $TiCl_4$ with titanium alkoxides in heptadecane (solvent) in the presence of TOPO (an additive or template). The alkoxide used would function as the oxygen donor for $TiCl_4$, and the alkyl groups of the alkoxide has to react with the chlorine, which needs a much higher reaction temperature (e.g., 300 °C) to form alkyl chloride products entering the liquid phase.[2]

At the stage of mixing $TiCl_4$ with acetone, $TiCl_4$ would assume the function of a Lewis acid to catalyze the well-known aldol condensation reaction of acetone to form diacetone alcohol, which can easily dehydrate to produce mesityl oxide and its isomers (Scheme 1). The dehydrated dimers could further condensate with the remaining acetone to produce varying amounts of dehydrated trimers, tetramers, etc.

On understanding the reactions occurring to the organic molecules, a plausible mechanism for the formation of TiO_2 materials in the present $TiCl_4$/Ac system could be given as Scheme 2. The water molecules required for hydrolysis of $TiCl_4$ were generated in situ by dehydration of the aldol condensation products as shown in Scheme 1. Hydrolysis of $TiCl_4$ would produce different $Ti(OH)_xCl_{4-x}$ species and volatile HCl because the ligand field strength of OH^- is higher than that of Cl^- ions. The occurrence of the hydrolysis reaction in this scheme was observed by color changes of the reaction solution and the release of a white acid fog (i.e., HCl) during the preparation of the reactant mixture. In the autoclaving stage at elevated temperatures (80−140 °C), the polycondensation of $Ti(OH)_xCl_{4-x}$ species would easily lead to extensive formation of the Ti−O−Ti network and then crystallization because the TiO_2 nanocrystals were formed during this autoclaving stage.

Our observation that single-phase rutile nanofibers are selectively produced at high $TiCl_4$ concentration (e.g., $TiCl_4$/Ac = 1/10 and 1/7) appears to agree with the known

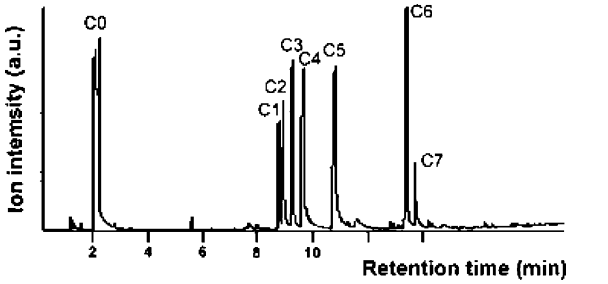

Figure 7. GC/MS plot of liquid products obtained from $TiCl_4$ and 4-methyl pentanone with a ratio of 1/30.

Scheme 3 [a]

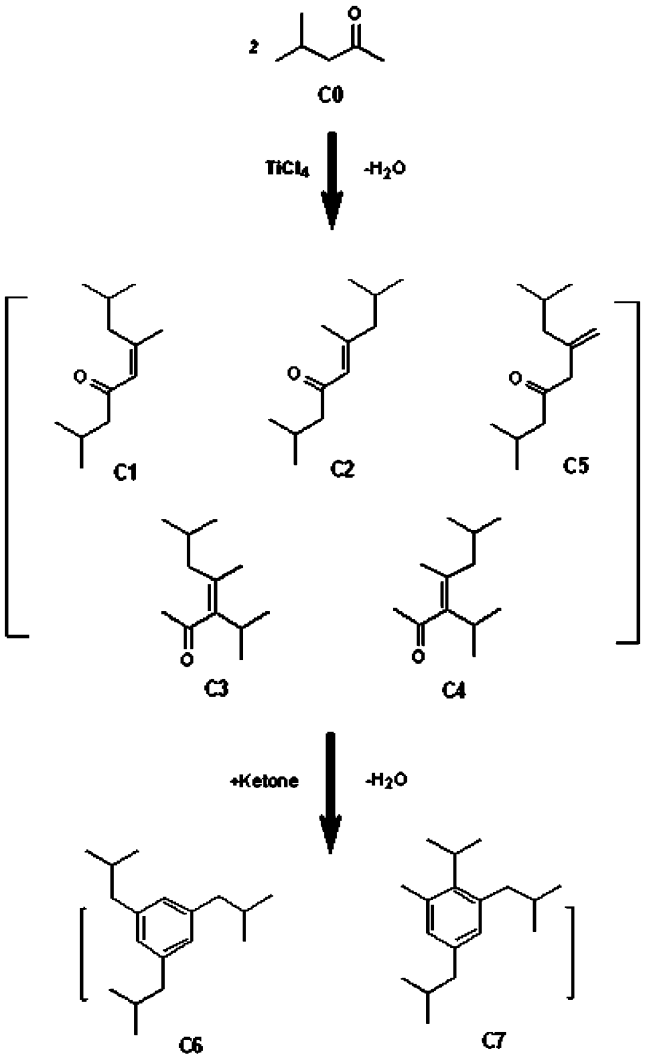

[a] Possible reactions leading to GC/MS-detected organics from the $TiCl_4$/4-methylpentanone mixtures. **C0**, **C1**, **C2**, ..., **C*n*** denote the organics detected in the liquids separated from the anatase product.

chemistry in many earlier syntheses of TiO_2 materials[12,13] that a strong acidity of the solution favors the formation of the rutile structure. When the $TiCl_4$ concentration is not high enough (e.g., $TiCl_4/Ac \leq 1/15$), acidity of the reaction system would be weak such that the formation and polycondensation of $Ti(OH)_xCl_{4-x}$ species would be slow. Thus, selective formation of the anatase particles is favored in the syntheses with lower reactant $TiCl_4/Ac$ ratios because the surface energy of an anatase particle is lower than that of a rutile one.[12]

With respect to the product morphology, we realized that there was no prior report on the formation of needlelike fibrous rutile materials in nonaqueous systems. It is speculated that the condensation products of acetone in the reaction system could play an important role in the morphology evolution of the rutile nanofibers.[14] Some of the high molecular weight condensation products, probably those of chlorine-containing ones, may assume the function of a template or protector in the formation of the fibrous rutile structure. However, we do not exclude the possibility that a faster hydrolysis step in the solution of strong acidity at high $TiCl_4/Ac$ ratios might also be a benefit to the fibrous morphology. It was shown earlier that the morphology of anatase materials obtained by controlled hydrolysis of titanium tetraisopropoxide in oleic acid was significantly affected by the modality of the water supply.[6,7] Fast addition of water induced rapid hydrolysis that gave TiO_2 nanorods as the product, whereas a slow supply of water produced nearly spherical particles.[7]

The dependences of the crystallite size and yield on the molar $TiCl_4/Ac$ ratio (Table 1) are indicative that the $TiCl_4/Ac$ ratio has a significant effect on the crystallite growth of the titania materials. The crystallite size and yield of titania materials also increase with the autoclaving temperature, suggesting that temperature is another parameter affecting crystallite growth. Compared with syntheses of anatase materials at low $TiCl_4$ concentration, the much-lower yield in producing fibrous rutile materials at high $TiCl_4$ concentration would hint a hindered growth of rutile crystals, probably because of the protection interaction of high molecular weight acetone condensates. Thus, autoclaving the reaction mixture of $TiCl_4/Ac = 1/10$ at 80 °C did not effect the formation of rutile materials (Table 1), but simply increasing the temperature to 140 °C resulted in growth of materials with continuously increased yield. It is expected that a further extension of the present approach for high-temperature synthesis would have the potential to generate titania nanostructures of larger dimensions.

Analysis of the organic products in the liquid phase of the autoclaved $TiCl_4$/ketone systems also demonstrated the occurrence of aldol condensation reactions of the alternative ketones. Figure 7 and Scheme 3 show examples of reactions when 4-methylpentanone was used as the reacting ketone. These data, together with those from other alternative ketones that are able to perform aldol condensation reactions (Table 2), are consistent with the mechanism discussed above.

4. Conclusions

Our data demonstrate that the technique of autoclaving $TiCl_4/Ac$ mixtures at 80−140 °C can be developed as a new approach for the synthesis of TiO_2 nanocrystallites with controlled crystal phase, size, and morphology. Single-phase anatase TiO_2 particles were obtained selectively when the $TiCl_4$ concentration is no higher than $TiCl_4/Ac = 1/15$, and fibrous rutile TiO_2 nanostructures were produced using mixtures with higher $TiCl_4$ concentrations. The particle size of the anatase crystallites increased with the $TiCl_4$ concentration and autoclaving temperature. The increase in the autoclaving temperature also significantly promoted the crystal growth of fibrous rutile nanostructures.

A plausible mechanism was proposed to account for the formation of single-phase TiO_2 nanostructures. At the beginning of the reaction, $TiCl_4$ functions as a Lewis acid to catalyze the aldol condensation of acetone. Dehydration of the acetone condensates produces water molecules, which induce the hydrolysis of $TiCl_4$ to $Ti(OH)_xCl_{4-x}$ species. During autoclaving at elevated temperature, the $Ti(OH)_xCl_{4-x}$ species condensate to form extensive Ti−O−Ti networks that grow to form single-phase nanostructures. This mechanism was also supported by our success in using other ketones as alternatives to acetone in synthesis.

Acknowledgment. The authors acknowledge financial support for this work from NSF (Grants 20573062 and 20590362), MOE (Grant SRFDP 20040003036), and the National Basic Research Program of China (Grant G2003CB-615804).

IC070199H

(12) Navrotsky, A. *Geochem. Trans.* **2003**, *4*, 34.
(13) (a) Park, H. K.; Kim, D. K.; Kim, C. H. *J. Am. Ceram. Soc.* **1997**, *80*, 743. (b) Kim, S.-J.; Park, S.-D.; Jeong, Y. H.; Park, S. *J. Am. Ceram. Soc.* **1999**, *82*, 927. (c) Cheng, H. M.; Ma, J. M.; Zhao, Z. G.; Qi, L. M. *Chem. Mater.* **1995**, *7*, 663. (d) Shin, H.; Jung, H. S.; Hong, K. S.; Lee, J. K. *Chem. Lett.* **2004**, *33*, 1382. (e) Li, Y. Z.; Fan, Y. N.; Chen, Y. *J. Mater. Chem.* **2002**, *12*, 1387.
(14) (a) Yin, H.; Wada, Y.; Kitamura, T.; Kambe, S.; Murasawa, S.; Mori, H.; Sakata, T.; Tanagida, S. *J. Mater. Chem.* **2001**, *11*, 1694. (b) Doxsee, K. M.; Cheng, R. C.; Chen, E.; Myerson, A. S.; Huang, D. P. *J. Am. Chem. Soc.* **1999**, *120*, 585.